Ultrasound in Med. & Biol., Vol. 47, No. 7, pp. 1747–1760, 2021

0301-5629/$ - see front matter

https://doi.org/10.1016/j.ultrasmedbio.2021.03.007

● *Original Contribution*

# FOCUSED ULTRASOUND-INDUCED BLOOD–SPINAL CORD BARRIER OPENING USING SHORT-BURST PHASE-KEYING EXPOSURES IN RATS: A PARAMETER STUDY

STECIA-MARIE P. FLETCHER,*,† MIN CHOI,* RANJITH RAMESH,* and MEAGHAN A. O'REILLY*,†

* Physical Sciences Platform, Sunnybrook Research Institute, Toronto, Ontario, Canada; and † Department of Medical Biophysics, University of Toronto, Toronto, Ontario, Canada

(*Received* 6 *January* 2021; *revised* 5 *March* 2021; *in final from* 12 *March* 2021)

**Abstract—Transient opening of the blood–spinal cord barrier has the potential to improve drug delivery options to the spinal cord. We previously developed short-burst phase-keying exposures to reduce focal depth of field and mitigate standing waves in the spinal canal. However, optimal short-burst phase-keying parameters for drug delivery have not been identified. Here, the effects of pressure, treatment duration, pulse length, burst repetition frequency and burst length on resulting tissue effects were investigated. Increased *in situ* pressures (0.23–0.33 MPa) led to increased post-treatment $T_1$-weighted contrast enhancement in magnetic resonance imaging ($p = 0.015$). Increased treatment duration (120 vs. 300 s) led to increased enhancement, but without statistical significance ($p = 0.056$). Increased burst repetition frequency (20 vs. 40 kHz) yielded a non-significant increase in enhancement ($p = 0.064$) but corresponded with increased damage observed on histology. No difference was observed in enhancement between pulse lengths of 2 and 10 ms ($p = 0.912$), corresponding with a sharp drop in the recorded second harmonic signal during the first 2 ms of the pulse. Increasing the burst length from two to five cycles (514 kHz) led to increased enhancement ($p = 0.014$). Results indicate that increasing the burst length may be the most effective method to enhance drug delivery. Additionally, shorter pulse lengths may allow more interleaved targets, and therefore a larger treatment volume, within one sonication. (E-mail: steciamarie.fletcher@mail.utoronto.ca)** 

*Key Words:* **Blood–spinal cord barrier, Focused ultrasound, Spinal cord, Trans-spinous ultrasound therapy.**

## INTRODUCTION

Blood vessels in the central nervous system include specialized features, termed the blood–brain barrier (BBB) and the blood–spinal cord barrier (BSCB), which limit molecular transport across the vascular endothelium. Free transport across these barriers is limited to lipid-soluble, small-molecule drugs with molecular weights less than 400–500 Da, and there are active transport mechanisms for essential nutrients (Pardridge 2005). Consequently, the majority of intravenously administered therapeutics are unable to efficiently penetrate the brain and spinal cord parenchyma, creating a roadblock to the effective treatment of diseases and disorders (Bartanusz et al. 2011; Daneman and Prat 2015).

Transient opening of these barriers mediated by focused ultrasound (FUS) and microbubbles provides an option for minimally invasive and targeted drug delivery (Hynynen et al. 2001), which can ultimately improve patient outcomes. In the brain, this technique has been expansively tested in pre-clinical studies for the delivery of tracers and therapeutics (Kinoshita et al. 2006; Choi et al. 2007; Jordão et al. 2010; Aryal et al. 2014), and has reached the stage of clinical trials in individuals with brain tumors (Carpentier et al. 2016; Mainprize et al. 2019), Alzheimer's disease (Lipsman et al. 2018) and amyotrophic lateral sclerosis (Abrahao et al. 2019). The feasibility of this technique for blood–spinal cord barrier opening (BSCBO) has been demonstrated in small animals (Wachsmuth et al. 2009; Weber-Adrian et al. 2015; Payne et al. 2017; O'Reilly et al. 2018; Fletcher et al. 2020b), in rabbits after laminectomy (Montero et al. 2019) and recently through the intact spine in pigs (Fletcher et al. 2020a).

At clinical scale, there are challenges to creating a uniform ultrasound focus within the spinal canal. At clinically relevant sub-megahertz frequencies, the dimensions of the

Address correspondence to: Stecia-Marie Fletcher, Physical Sciences Platform, Sunnybrook Research Institute, 2075 Bayview Avenue, Room M7-302, Toronto, Ontario M4N 3M5, Canada. E-mail: steciamarie.fletcher@mail.utoronto.ca

ultrasound focus are long compared with those of the spinal canal. This is compounded by reflective boundary conditions imposed at the walls of the spinal canal, which lead to the formation of standing waves, compromising treatment safety and efficacy (Daffertshofer et al. 2005; Baron et al. 2009). We previously developed a dual-aperture approach and a pulse sequence of closely timed, randomly phased short bursts; called short-burst phase keying (SBPK), which reduces the focal depth of field and mitigates the formation of standing waves in *ex vivo* human vertebrae (Fletcher and O'Reilly 2018). This approach has been successful in achieving targeted and uniform BSCBO in rats (Fletcher et al. 2020b), and in pigs through the intact vertebral arch (Fletcher et al. 2020a).

SBPK exposure parameters have been specifically tailored to overcome clinical-scale technical challenges, but there is currently no understanding of the impact of parameters such as burst length and burst repetition frequency (BRF) on the efficacy of BSCBO. Adjusting these parameters may have significant implications for drug delivery. Previous parameter studies, using pulses on the order of milliseconds, have highlighted the importance of factors like duty cycle on the threshold and magnitude of BBB opening (BBBO; McDannold et al. 2008; Chopra et al. 2010). These have played an essential role in developing the standard range of parameters currently used in pre-clinical and clinical testing. While parameter studies using short-burst exposures in the absence of phase modulations for BBBO have previously been published (Choi et al. 2011; O'Reilly et al. 2011), the implications for translation to the spinal cord are not understood.

In this study, we investigated the effects of acoustic pressure, total treatment duration, burst-train (pulse) length, BRF and burst length when using SBPK FUS for BSCBO. *In vivo* results from 20 rats (plus four sham rats) are presented, and their implications for the optimization of BSCBO are discussed. The findings presented here will be used to tailor the design of SBPK FUS exposures for future studies.

## MATERIALS AND METHODS

### *Dual-aperture approach and SBPK*

In this work, FUS was generated using two in-house, spherically focused, confocal, lead zirconate titanate 1-3 piezocomposite transducers (elements sourced from DeL Piezo Specialties, LLC, West Palm Beach, FL, USA) in a cross-beam approach to reduce the focal size (Sun et al. 2017a; Fletcher and O'Reilly 2018), as shown in Figure 1a. The transducers used had a center frequency $f_0 = 514$ kHz, diameter = 50 mm, and focal length = 60 mm, and were

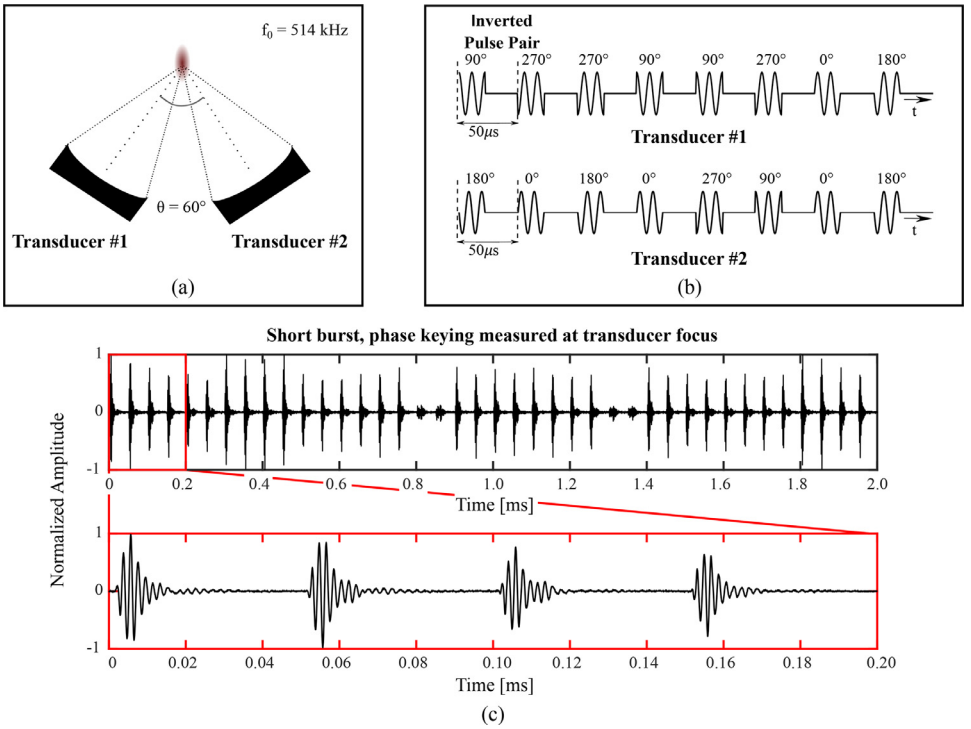


Fig. 1. (a) Schematic diagram of the dual-aperture approach used for reducing focal depth of field. Transducers have a center frequency of 514 kHz, aperture diameter of 50 mm, and focal length of 60 mm. (b) Example of the short-burst phase-keying pulses used to drive each transducer. These pulses allow the formation of a uniform focus in the vertebral canal at clinical scale, without standing waves or grating lobes. (c) Normalized amplitude of short-burst phase-keying pulse measured at the focus of the transducers, using a needle hydrophone.

separated by 60°. The focal dimensions, as defined by the 70% maximum pressure contour, were approximately 3.0 mm laterally and 5.5 mm axially. The transducers were matched to 50 Ω, 0° using external matching circuits. A dual-channel arbitrary-function generator (AFG 31000 Series, Tektronix, Beaverton, OR, USA) and two 53 dB radio-frequency power amplifiers (NP-2519, NP Technologies Inc., Newbury Park, CA, USA) were used to drive the transducers. The peak negative pressure achieved at the focus using SBPK exposures was calibrated by performing acoustic field scans in a tank of de-gassed and de-ionized water using a 0.5 mm polyvinylidene difluoride needle hydrophone (Precision Acoustics, Dorchester, UK).

SBPK exposures as shown in Figure 1b were used to achieve BSCBO (Fletcher and O'Reilly 2018; Fletcher et al. 2020b). SBPK pulses were generated in MATLAB (2016a, The MathWorks, Natick, MA, USA) and uploaded to the arbitrary-function generator. In previous work by our group, and for the control FUS treatments in this study, these excitations consisted of short bursts, with burst length = 2 cycles (transducer response = 4.5 $\mu$s) and burst repetition period = 50 $\mu$s (BRF = 20 kHz). The short burst length was necessary to mitigate the formation of standing waves in the spinal canal. To avoid the formation of grating lobes at the focus of the two transducers, pseudo-random phases were applied at the start of each burst. Independently for each transducer, odd-numbered bursts were assigned a random quadrature phase (0°, 90°, 180°, 270°), and even-numbered bursts were 180° phase-inverted from the previous burst so that pulse inversion could be used in the analysis of acoustic emissions from microbubbles during FUS treatments (Simpson et al. 1999; Fletcher and O'Reilly 2018). An example of a pulse measured at the focus of the transducers is shown in Figure 1c.

*Animal preparation and FUS treatments*

Animal experiments were approved by the Sunnybrook Research Institute Animal Care Committee and were performed in keeping with guidelines from the Canadian Council on Animal Care. Twenty-four Sprague Dawley rats (12 male, 259−573 g; 12 female, 199−464 g; Charles River Laboratories, Wilmington, MA, USA) were used for these experiments. Animals were anesthetized using 2% isoflurane and oxygen, and before the ultrasound exposures the carrier gas was switched to medical air (McDannold et al. 2017). The hair on the backs of the animals was removed using an electric razor, followed by a depilatory cream, to improve acoustic coupling between the transducers and the skin.

The dual-aperture transducer setup was mounted on a 3-D positioning arm, contained within the water bath of small-animal pre-clinical ultrasound treatment platform (RK-100, FUS Instruments, Toronto, Ontario, Canada). An in-house-fabricated, unfocused, 5 mm diameter lead zirconate titanate receiver (elements sourced from DeL Piezo Specialties) with a center frequency of 250 kHz (near the subharmonic $f_0/2$) was roughly aligned with the focus of the transducers and used to receive acoustic emissions from microbubbles during treatments. A 125 MS/s 14-bit Peripheral Component Interconnect digitizer (ATS460, Alazar Technologies Inc., Pointe-Claire, Quebec, Canada) was used to capture receiver signals at a sampling rate of 20 MS/s, and data were processed in MATLAB. A diagram showing the setup for *in vivo* experiments is shown in Figure 2a.

The height of the focus with respect to the RK-100 system was determined by raising the water level to a pre-calibrated level in a phantom. A fountain was

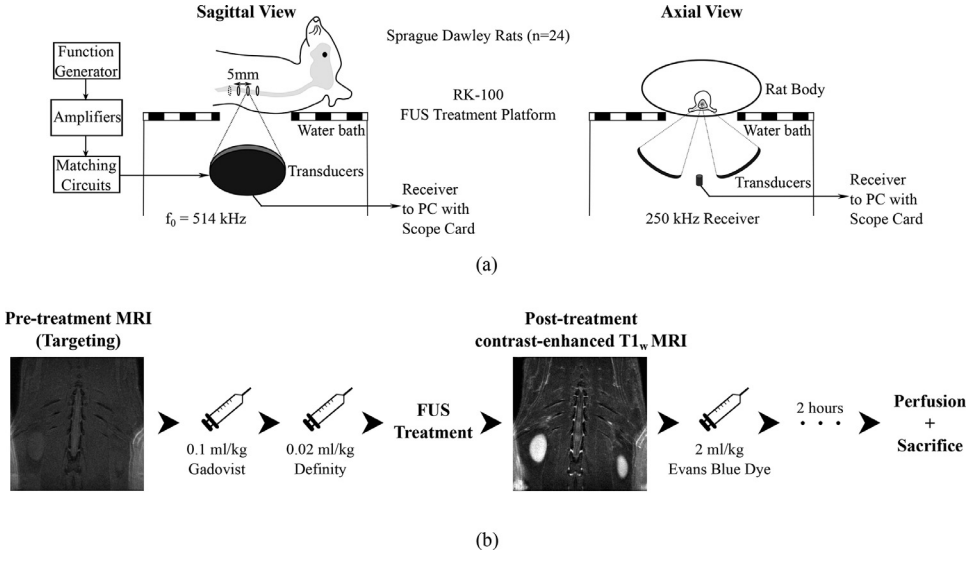


Fig. 2. (a) Schematic diagram showing sagittal and axial views of the experimental setup used for focused ultrasound treating animals using the RK-100 pre-clinical treatment platform. (b) Workflow used for treating each animal.

generated at the water surface by transmitting with a continuous wave. The water level was adjusted ±2 mm to maximize the fountain height, and this was set as the focal length. The position of the focus in the transverse plane was marked with a magnetic resonance imaging (MRI)-compatible fiducial marker. The phantom was imaged in the bore of an MRI scanner (Biospec 7 T, Bruker Co., City, MA, USA), and the coordinates of the focus were co-registered between the scanner and the treatment system.

A treatment timeline for each animal is shown in Figure 2b. Animals were placed supine on the FUS delivery system. Three or four targets (5 mm spacing) in the lower thoracic region of the spinal cord were chosen under $T_1$-weighted MRI guidance (Fast spin echo, field of view = 6 × 6 cm, spatial discretization = 0.3 mm, slice thickness = 0.5 mm, echo time = 5.5 ms, repetition time = 500 ms, rare factor = 4, number of averages = 12) and sonicated using SBPK FUS at fixed acoustic pressures. Microbubbles (0.02 mL/kg Definity, Lantheus Medical Imaging, MA, USA) were administered intravenously through the tail vein, as a bolus, at the start of the sonication. This microbubble dose corresponds to twice the recommended clinical bolus dose indicated on the product fact sheet. Exposures were interleaved so that all targets were treated during a single sonication—that is, requiring a single injection of microbubbles—except in the groups where BRF and burst length were investigated, where two injections were used, separated by at least 5 min.

To confirm BSCBO, coronal $T_1$-weighted, contrast-enhanced MRI (0.1 mL/kg, Gadovist, Bayer Inc., Mississauga, Ontario, Canada) was performed immediately after sonications. BSCBO was considered successful if the mean MRI signal in a 3 × 3 voxel area centered on maximum enhancement was at least two standard deviations greater than the mean signal in a baseline 3 × 3 voxel unsonicated area in the spinal cord. MRI images were analyzed using Medical Image Processing, Analysis and Visualization (National Institutes of Health, Bethesda, MD, USA). After treatments, Evans blue dye (4% weight per volume saline dilution, 2 mL/kg; Thermo Fisher Scientific, Waltham, North Billerica, MA, USA) was administered intravenously through the tail vein to verify BSCBO and locate treatment locations after tissue harvesting.

Approximately 2 h after FUS sonication, spinal cords were formalin fixed through trans-cardial perfusion with saline followed by 10% neutral buffered formalin under deep anesthetic, and harvested for histological staining. Coronal sections 5 $\mu$m thick at 100 $\mu$m intervals were stained using hematoxylin and eosin and evaluated for tissue damage. Tissue damage at each treatment location was evaluated using a four-point grading scheme adapted from Hynynen et al. (2005) as described in Table 1. Grading was done by a researcher who was unaware of treatment parameters.

Table 1. Descriptions of grades used to assess damage at target locations in histology

| Grade | Description |
|---|---|
| 0 | No damage on any histology level |
| 1 | Very minor damage—one to a few very small clusters of red blood cells on at least one histology level |
| 2 | Moderate (more significant) damage—one larger cluster of red blood cells or a greater number of small clusters of red blood cells on at least one histology level |
| 3 | Extensive damage—a large number of clusters of red blood cell extravasation, with or without pooling on at least one histology level |

*SBPK sonication parameters*

Each SBPK treatment consisted of pulses comprising short bursts, which were repeated with a pulse repetition frequency of 1 Hz over some total treatment duration (Fig. 3). The SBPK parameters investigated for BSCBO were acoustic pressure, total treatment duration, burst-train (pulse) length, BRF and burst length (Fig. 3). The set of control parameters was based on previous work with SBPK pulses (Fletcher and O'Reilly 2018; Fletcher et al. 2020b) and on established values used for BBBO (McDannold et al. 2008; Chopra et al. 2010). The control pulse had total treatment duration = 120 s, pulse length = 10 ms, BRF = 20 kHz, burst length = 2 cycles (duty cycle = 0.0008%) and estimated *in situ* peak negative pressure = 0.28 MPa. *In situ* pressure estimates were based on a mean pressure transmission of 67% ± 15% through the rat spine at 551.5 kHz (O'Reilly et al. 2018). Animals were divided into six groups: one for each parameter investigated and an additional sham group, where microbubbles were not administered. Table 2 shows the distribution of animals

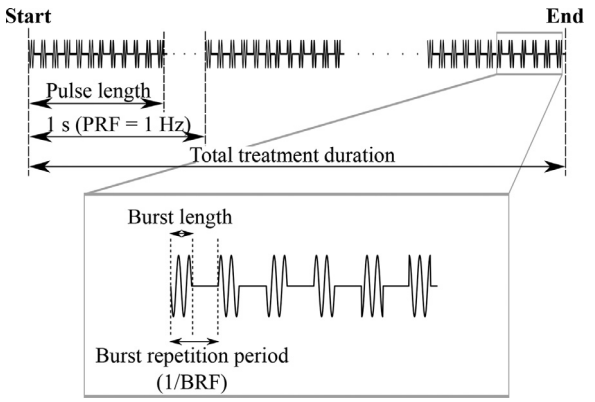


Fig. 3. Parameters investigated during this study: treatment duration, pulse length, burst repetition frequency (BRF) and burst length.

Table 2. Parameters of short-burst phase keying tested in this study and how they were varied between animals

| Variable | Sham | Acoustic pressure (MPa) | Treatment duration (s) | Pulse length (ms) | Burst repetition frequency (kHz) | Burst length (cycles) |
|---|---|---|---|---|---|---|
| Values tested | N/A | 0.23, **0.28**, 0.33 | **120**, 300 | 2, **10** | **20**, 40 | **2**, 5 |
| Locations per animal | 3 | 3 | 3 | 3 | 4 | 4 |
| Number of animals (M/F) | 4 (1/3) | 4 (2/2) | 4 (2/2) | 4 (2/2) | 4 (3/1) | 4 (2/2) |

Boldface indicates control parameters.

in each group, as well as the values of the parameters investigated, and Figure 4 illustrates how each parameter was varied by spinal cord location in each group.

*Sham animals*

To confirm that BSCBO occurred as a result of the mechanical action of microbubbles and not of thermal effects, 4 rats (3 female, 1 male, 214−344 g) were treated at three locations per spinal cord, using control parameters with FUS only (Fig. 4a).

*Pressure group*

To investigate the effect of acoustic pressure, 4 rats (two female, two male, 326−551 g) were treated at three locations per spinal cord. The acoustic pressures chosen were near the lower threshold observed for BSCBO using SBPK FUS in our previous work (Fletcher et al. 2020b). Three pressure levels (estimated *in situ* pressure = 0.23, 0.28 and 0.33 MPa) were investigated sequentially in each animal (Fig. 4b).

*Total treatment duration group*

To determine whether increasing the treatment duration from 120 to 300 s would have an effect, 4 rats (2 female, 2 male, 199−573 g) were treated at three locations per spinal cord. Treatment durations of 120 and 300 s were tested within each animal (Fig. 4c).

*Pulse length group*

To investigate the effect of pulse length, 4 rats (2 female, 2 male, 206−542 g) were treated at three locations per spinal cord. The pulse lengths tested were 2 ms and the control pulse length of 10 ms. Both pulse lengths were tested in each animal (Fig. 4d).

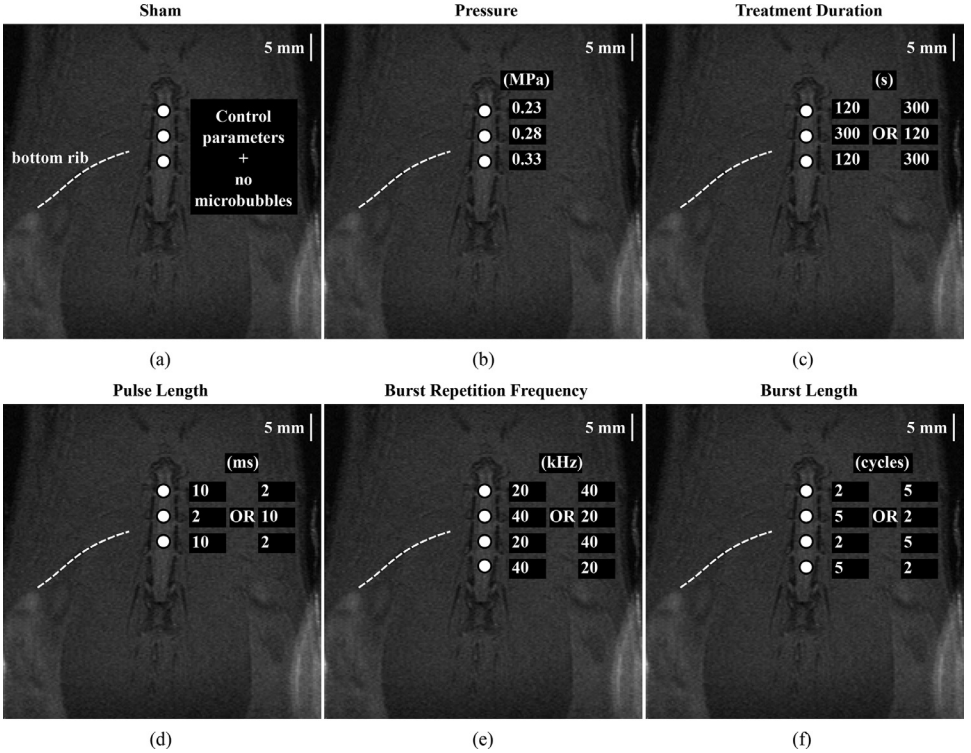


Fig. 4. Variation of short-burst phase-keying parameters by location in (a) the sham group, (b) the pressure group, (c) the treatment duration group, (d) the pulse length group, (e) the burst repetition frequency (BRF) group, and (f) the burst length group.

*BRF group*

To determine whether increasing the BRF would affect BSCBO, 4 rats (1 female, 3 male, 221−290 g) were treated at four locations per spinal cord. BRFs of 20 and 40 kHz were tested in each animal (Fig. 4e). Technical limitations of the arbitrary-function generator meant that the BRF could not be interleaved in one treatment. To overcome this, two locations 10 mm apart were treated with the first BRF. A second treatment, with a second injection of microbubbles, was then performed with the second BRF, for a total of four locations at 5 mm spacing. There was a minimum of 5 min between treatments, to allow for the bubbles from the first injection to clear. The gadolinium contrast agent was administered as a bolus at the start of the second treatment. To account for potential differences in enhancement owing to the time of gadolinium administration, the order in which the two BRFs were administered was varied among the animals. This also allowed for the treatment of an additional treatment location in this group.

*Burst length group*

To investigate the effect of burst length, four rats (2 female, 2 male, 206−542 g) were treated at four locations per spinal cord. The burst lengths tested were 5 cycles and the control pulse length of 2 cycles. Both pulse lengths were tested in each animal, requiring two injections, similar to the BRF group (Fig. 4f). Figure 5 shows normalized measured bursts at the focus for both burst lengths investigated. The temporal burst lengths, as defined by the full-width at half maximum of the burst envelopes, were 4.5 and 10.5 $\mu$s, respectively, for 2-cycle and 5-cycle driving bursts. To account for transducer ramp-up time, focal pressures were calibrated independently for the two burst lengths, and driving voltages were adjusted to allow the same resultant focal peak negative pressures. Using the same driving voltage from the arbitrary-function generator, 5-cycle bursts resulted in 28% higher peak negative pressures than 2-cycle bursts.

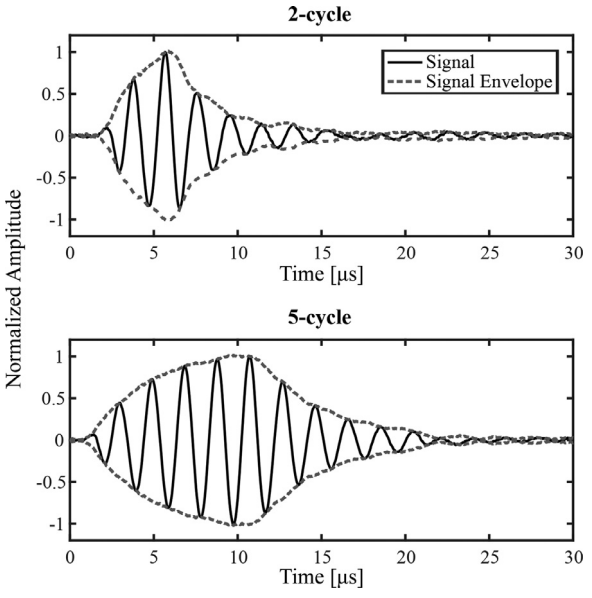


Fig. 5. Normalized amplitude of a single short-burst phase-keying burst, measured using a needle hydrophone at the focus of the transducers, for 2-cycle and 5-cycle driving bursts.

*Statistical analysis*

Statistical analyses were computed in R (version 4.0.3), and a one-way analysis of variance (ANOVA) was used to determine statistical differences among parameters. In treatment groups where just two parameter values were tested, this method was chosen in preference to the *t*-test because it could account for incomplete pairing within test subjects. In groups where more than two parameter values were tested, a *t*-test with equal variance was computed *post hoc*, without adjusting for multiple comparisons (Rothman 1990). For all analyses, a $p$ value of 0.05 was used as the threshold for statistical significance.

*Acoustic data analysis*

Acoustic data analysis was performed in MATLAB as described in our previous work using SBPK exposures (Fletcher et al. 2020b). Before each treatment, baseline measurements were made of received acoustic signals, in the absence of microbubbles, throughout the total treatment duration. Baseline and treatment acoustic data were divided into short time windows, shorter in length than the burst repetition period (BRF = 20 kHz, window length = 35 $\mu$s; BRF = 40 kHz, window length = 17$\mu$s). The start time of these windows was selected based on the predicted time of flight from the focus of the transducers to the receiver. After windowing, the received signals from consecutive, inverted bursts were added together in the time domain to use pulse inversion. Next, the resultant time-domain signals were converted to frequency spectra using a Fourier transform. Maximum projections in the frequency domain were performed over the pulse length and total treatment duration to capture any changes that occurred. Finally, a ratio was taken between treatment and baseline data.

The frequencies of interest were the second harmonic ($2f_0$ = 1028 kHz) and the subharmonic ($f_0/2$ = 257 kHz). Quantitative analyses of peaks occurring at these frequencies was performed by considering the area under a 57 kHz region of interest, centered on these frequencies.

*Benchtop experiments*

Adjusting some parameters, specifically the BRF and burst length, has the potential to adversely affect SBPK's efficacy at standing-wave mitigation in the human vertebral canal. Therefore, trans-spinous benchtop field measurements

were performed for consequential parameters that were observed to increase BSCBO *in vivo*. Benchtop experiments were performed in a tank of de-gassed and de-ionized water which was maintained at 37°C. The transducer setup was the same as in the *in vivo* experiments. The focus of the transducers was found by using a 0.5 mm polyvinylidene difluoride hydrophone to measure the time-domain acoustic field data. The hydrophone was navigated using a 3-D positioning system (Velmex Inc., Bloomfield, NY, USA). Data acquired with the hydrophone were displayed on a mixed-domain oscilloscope (MDO3014, Tektronix) and subsequently transferred to a PC, where they were stored and saved. The data were processed in MATLAB to visualize the temporal peak pressure distribution for the ultrasound field, and the location at which the maximal pressure was measured was used to determine the focus.

Trans-spinous measurements were performed through the posterior elements of three *ex vivo* thoracic vertebrae (T1, T5, T12) from an adult human spine (Osta International, White Rock, British Columbia, Canada). Vertebrae were de-gassed in a vacuum jar over several weeks to remove trapped gas, and for a minimum of 2 h immediately before experiments. Once immersed in the water tank, the vertebrae were allowed to sit for 1 h before measurements were made, to allow for thermal equilibrium at 37°C. Measurements were performed within an 8 × 8 mm field of view, with the focus of the transducers centered within the vertebral canal.

*Effects of biological sex and subject weight*

Thirty-two locations across 20 rats (9 female, 11 male, 199–573 g) were treated using the control SBPK parameters. For these locations, a one-way ANOVA was used to determine whether there was a statistically significant difference ($p < 0.05$) in MRI enhancement or weight between male and female rats. Statistically significant differences in animal weight between males and females were also considered, as these may be a compounding factor. A linear regression was used to model the relationship between MRI enhancement and animal weight. All statistical analyses were performed in R.

## RESULTS

*Sham group and BSCBO*

No evidence of BSCBO through MRI enhancement or extravasation of Evans blue dye was observed in animals in the sham group (without microbubbles). Figure 6 shows representative examples of post-treatment, coronal $T_1$-weighted contrast-enhanced MRI compared with other treatment groups. In all four animals in the sham group, no adverse effects were observed in histology, and all treatment locations were graded as grade 0.

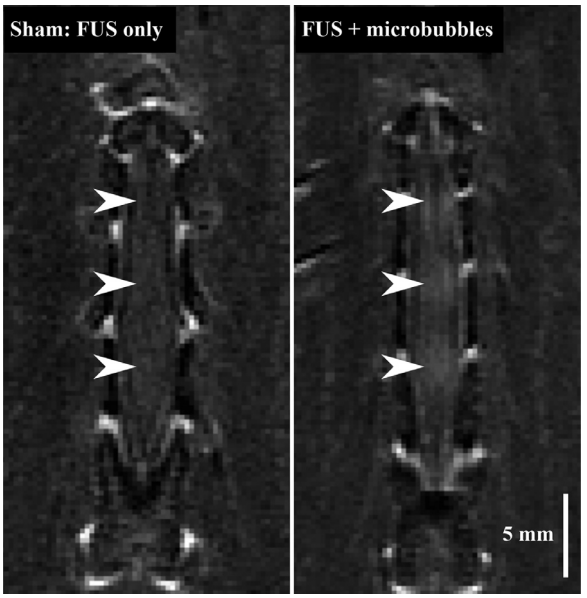


Fig. 6. Representative post-treatment $T_1$-weighted, contrast-enhanced magnetic resonance images comparing enhancement in (left) the group with focused ultrasound only and (right) other treatment groups using focused ultrasound and microbubbles (taken from the pulse-length group). The white arrows indicate the target treatment locations.

*Histology grades*

A range of histology scores were assigned across treatment locations. Figure 7 shows representative images of observed tissue damage at treatment locations, corresponding to the grades described in Table 1.

*Pressure group*

The key findings are outlined in Table 3. MRI enhancement at treatment locations showed an increasing trend with increasing estimated *in situ* peak negative pressure (Fig. 8). The mean ± standard deviation (SD) MRI enhancement (with range) was 17.8% ± 4.9% (10.9%–22.4%), 25.9% ± 9.8% (13.0%–35.3%) and 33.9% ± 8.8% (21.9%–41.1%), respectively, for *in situ* pressure estimates of 0.23, 0.28 and 0.33 MPa. At the lowest pressure investigated, MRI enhancement above baseline was insufficient to qualify as BSCBO, as defined by this study. The one-way ANOVA resulted in a $p$ value of 0.015, indicating statistically significant differences between the pressures tested. Using *post hoc* paired $t$-tests, we found statistical significance between locations treated with 0.23 and 0.33 MPa ($p = 0.035$) and those treated with 0.28 and 0.33 MPa ($p = 0.002$). Despite an increasing trend with acoustic pressure, no statistical significance was found between groups treated with 0.23 and 0.28 MPa ($p = 0.190$). In one animal, an anomaly occurred, with the location treated with 0.23 MPa showing greater enhancement than the location treated with 0.28 MPa—potentially a result of the sound penetrating

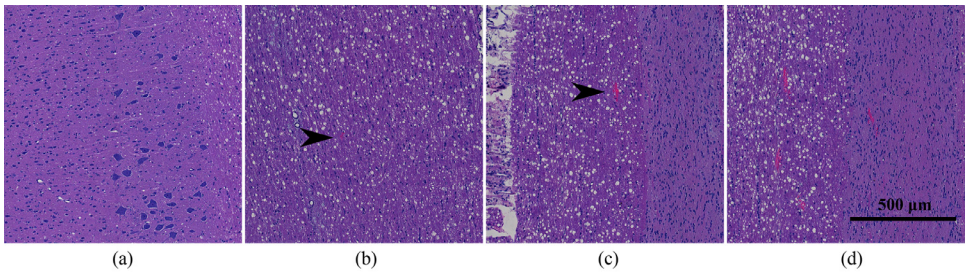


Fig. 7. Representative images of tissue effects observed at histology, corresponding to the grading scale described in Table 1: (a) grade 0—no damage, (b) grade 1—minor damage, (c) grade 2—moderate damage and (d) grade 3—extensive damage. Arrows indicate regions of red blood cell extravasation.

Table 3. Key findings of the effects of various parameters on blood–spinal cord barrier opening

| Parameter | Values tested | % MRI enhancement (mean ± SD) | | | $p$* | Notes |
|---|---|---|---|---|---|---|
| | | Value 1 | Value 2 | Value 3 | | |
| Pressure (MPa) | 0.23, **0.28**, 0.33 | 17.8 ± 4.9 | 25.9 ± 9.8 | 33.9 ± 8.8 | 0.015† | |
| Treatment duration (s) | **120**, 300 | 22.2 ± 2.8 | 29.5 ± 8.7 | N/A | 0.056 | |
| Pulse length (ms) | 2, **10** | 27.9 ± 8.4 | 29.9 ± 8.1‡ | N/A | 0.912 | |
| Burst repetition frequency (kHz) | **20**, 40 | 24.7 ± 7.9 | 31.9 ± 9.8 | N/A | 0.064 | Increased evidence of red blood cell extravasation with increasing burst repetition frequency |
| Burst length (cycles) | **2**, 5 | 29.3 ± 4.5 | 38.0 ± 6.6 | N/A | 0.014† | |

* One-way analysis of variance.
† Statistically significant ($p < 0.05$).
‡ Outlier removed.

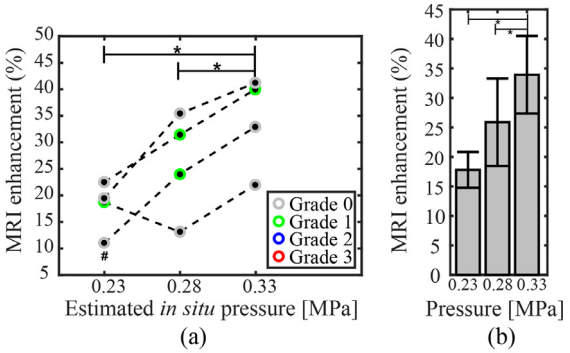


* : p < 0.05
# : insufficient evidence of BSCBO

Fig. 8. (a) Magnetic resonance imaging enhancement and histology grade at each treatment location across the different peak negative pressures investigated. (b) Mean enhancement achieved across the pressures investigated, with error bars indicating the inter-quartile range.

a more favorable acoustic window. All treatment locations in this group were graded 0 or 1 at histology, and no differences were observed between the different pressures.

*Total treatment duration group*

The key findings are outlined in Table 3. The mean ± SD MRI enhancement (with range) was 22.2% ± 2.8% (18.8%–25.7%) at locations treated for 120 s and 29.5% ± 8.7% (21.3%–40.5%) for a treatment duration of 300 s (Fig. 9). Despite increased MRI enhancement at 300 s compared with 120 s in three out of four animals in this group, no statistical difference between the durations was identified using a one-way ANOVA ($p = 0.056$), although significance might be achieved with a larger group size. All treatment locations in this group were graded 0 or 1 at histology, and no differences in histological damage were observed between the two treatment durations.

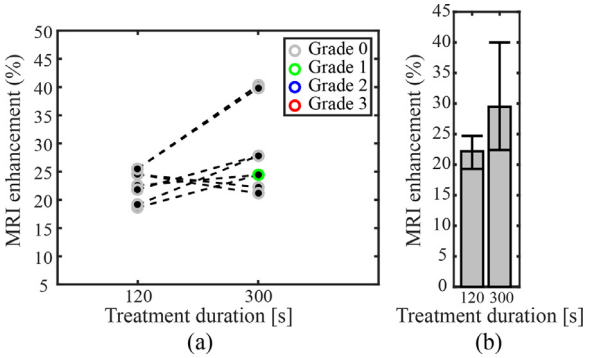


Fig. 9. (a) Magnetic resonance imaging enhancement and histology grade at each treatment location between the two treatment durations investigated. (b) Mean enhancement achieved for the two treatment durations, with error bars indicating the inter-quartile range.

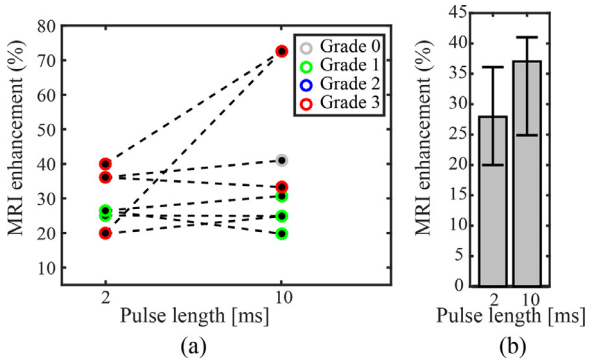


Fig. 10. (a) Magnetic resonance imaging enhancement and histology grade at each treatment location between the two pulse lengths investigated. (b) Mean enhancement achieved for the two pulse lengths, with error bars indicating the inter-quartile range.

*Pulse length group*

The key findings are outlined in Table 3. The mean ± SD MRI enhancement (with range) was 27.9% ± 8.4% (19.8%−40.0%) at locations treated with a pulse length of 2 ms and 37.0% ± 18.8% (19.8%−72.5%) for a pulse length of 10 ms (Fig. 10). There was one outlier at a location treated with a pulse length of 10 ms, with an MRI enhancement of 72.5%. Removing this outlier led to a mean ± SD MRI enhancement (with range) of 29.9% ± 8.1% (19.8%−41.0%) for the 10 ms pulse length. After the outlier was excluded, there was no trend observed between locations treated with the two treatment durations. A one-way ANOVA showed no statistical significance between the pulse lengths ($p = 0.912$). In two rats, extensive (grade 3) damage was observed, independent of pulse length, at five of six locations. Evidence of cavitation activity at the subharmonic was observed at three of these locations, but not in either of the remaining animals in this group. This is indicative of FUS overexposure, owing to higher-than-expected *in situ* pressures in these animals.

Considering the microbubble activity within each burst train of short bursts in SBPK FUS, it was found that microbubble activity at the second harmonic dropped off within the first 2 ms of a 10 ms burst train. A representative example of this effect is shown in Figure 11. This effect was frequently observed at treatment locations throughout all treatment groups (76% of locations where a distinct peak at the second harmonic was observed) and is thought to contribute to the lack of differences in MRI enhancement observed here.

*BRF group*

The key findings are outlined in Table 3. The mean ± SD MRI enhancement (with range) was 31.1% ± 9.8% (14.5%−42.2%) in animals treated with a BRF of

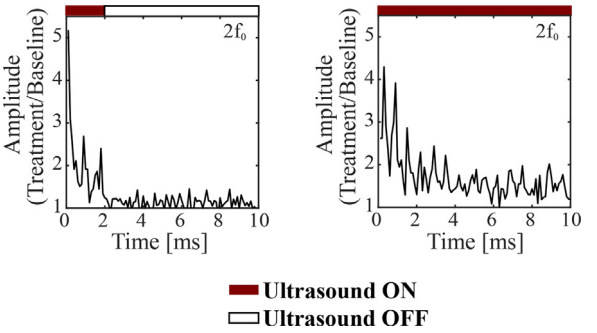


Fig. 11. Representative recorded bubble activity at the second harmonic ($2f_0$), expressed as a ratio between treatment and baseline data for (left) 2 ms pulse lengths and (right) 10 ms pulse lengths, for locations in the same animal.

40 kHz, compared with 24.7% ± 7.9% (16.1%−37.3%) in animals treated with the control BRF of 20 kHz (Fig. 12). While there was a trend of increased MRI enhancement with increased BRF, a one-way ANOVA failed to identify statistical significance ($p = 0.064$). However, grade 2 damage was observed at four out of eight locations treated at the higher BRF (occurring in three of four animals), compared with one out of eight at the lower BRF, indicating the potential for increased adverse tissue effects with the increased BRF. No differences in the acoustic cavitation signals were observed between the two BRFs.

*Burst length group*

The key findings are outlined in Table 3. The mean ± SD MRI enhancement (with range) was 29.3% ± 4.5% (22.6%−34.2%) in animals treated with 2-cycle bursts and 38.0% ± 6.6% (25.4%−46.9%) in animals treated with 5-cycle bursts (Fig. 13). A one-way

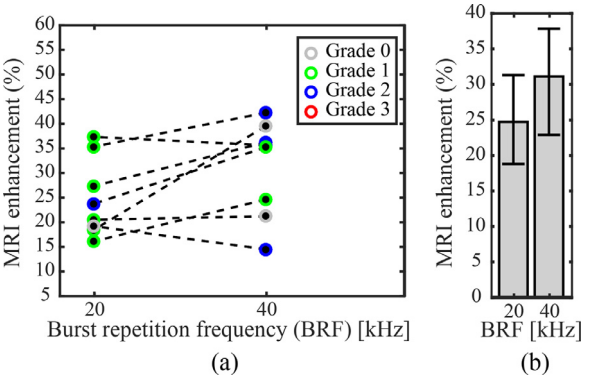


Fig. 12. (a) Magnetic resonance imaging enhancement and histology grade at each treatment location between the two burst repetition frequencies investigated. (b) Mean enhancement achieved for the two burst repetition frequencies, with error bars indicating the inter-quartile range.

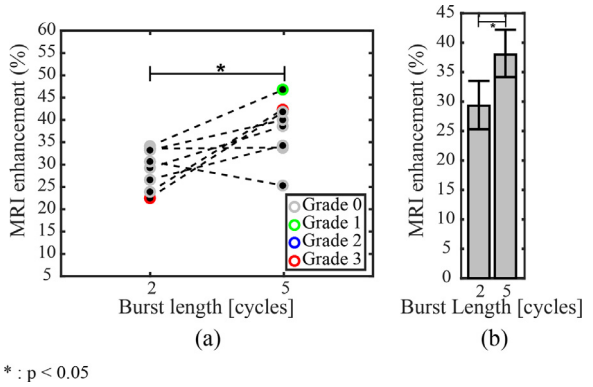


Fig. 13. (a) Magnetic resonance imaging enhancement and histology grade at each treatment location between the two burst lengths investigated. (b) Mean enhancement achieved for the two burst lengths, with error bars indicating the inter-quartile range.

ANOVA found that the resultant MRI enhancement was statistically significant ($p = 0.014$). Most treatment locations in this group were graded 0 or 1 at histology, and no differences in histological damage were observed between the two burst lengths. In one subject, extensive (grade 3) damage was observed, independent of pulse length, at two of four locations in the spinal cord. Evidence of cavitation activity at the subharmonic was observed at one of these locations, but not in any of the remaining animals in this group. This is indicative of FUS over-exposure, owing to higher-than-expected *in situ* pressures in these animals.

While this is a promising result for improving therapeutic delivery, increasing the burst length has the potential to minimize the efficacy of SBPK FUS at mitigating standing waves in human vertebrae. Benchtop measurements were performed at the focus of the dual-aperture setup for two positions of the vertebrae relative to the transducers. These measurements indicated that increasing the burst length to 5 cycles while maintaining other parameters at their control values led to focal distortion owing to standing waves near the wall of the vertebral body (Fig. 14). These standing waves were qualitatively not as pronounced as those observed in our previous work with longer burst (30-cycle) exposures (Fletcher and O'Reilly 2018). However, decreasing the BRF from the control value of 20 kHz (period = 50 $\mu$s) to 18.2 kHz (period = 55 $\mu$s) and then to 16.7 kHz (period = 60 $\mu$s) minimized standing waves near the vertebral body wall (Fig. 14). The long delay between bursts required to reduce standing waves suggests that the sound undergoes multiple non-negligible reflections within the canal before attenuating sufficiently so as to not interfere with the subsequent burst.

*Effects of biological sex and subject weight*

One outlier location (enhancement = 72.5%) was excluded from statistical analysis, leaving 31 locations

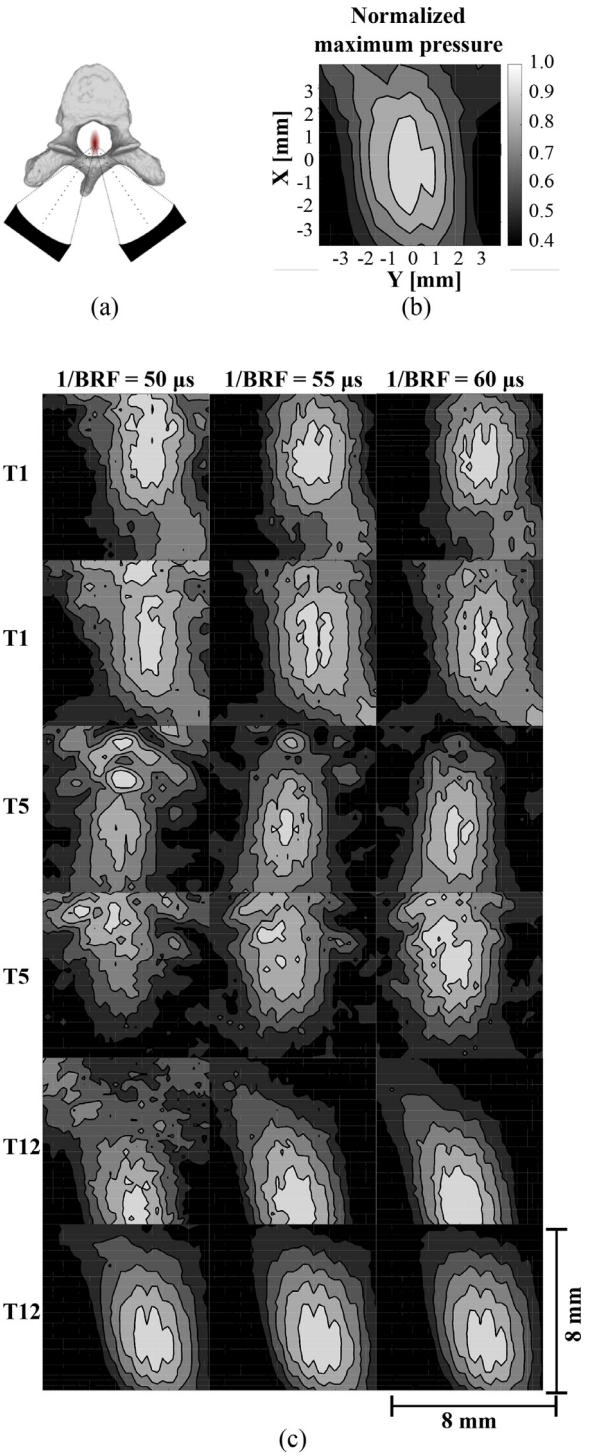


Fig. 14. (a) Schematic diagram showing the orientation of the transducers relative to the vertebrae in benchtop measurements. (b) 2-D plot of the normalized maximum pressure distribution measured at the focus of the transducers in free field (water). (c) Normalized maximum pressure plots at the free-field focus for two transducer–vertebrae orientations in three thoracic vertebrae (T1, T5, T12), showing the effect of burst-repetition frequency on standing-wave formation.

across 19 Sprague-Dawley rats (eight female, 11 male, 199−573 g) that were treated using the control SBPK parameters. The mean ± SD MRI enhancement (with range) was 23.9% ± 6.9% (13.0%−35.6%) in male rats and 31.5% ± 6.8% (19.3%−42.2%) in females. A one-way ANOVA showed statistical significance in the MRI enhancement between male and females treated with control parameters ($p = 0.037$). However, there was also a difference in weights between the male and female animals, with the mean ± SD weight (with range) of the male rats being 421 ± 134 g (269−573 g) and that of the females being 259 ± 92 g (199−464g). A one-way ANOVA showed that the difference in weights was statistically significant ($p = 0.006$), but a linear regression indicated poor correlation between animal weight and MRI enhancement ($R^2 = 0.10$), as shown in Figure 15.

## DISCUSSION

In this study, we aimed to identify the influence of SBPK FUS sonication parameters of pressure, treatment duration, pulse length, burst length and BRF on BSCBO. Increased acoustic pressure and burst length led to statistically significant increases in MRI contrast enhancement at target locations (pressure: $p = 0.015$; burst length: $p = 0.014$). At the values tested in this study, increasing these parameters was not shown to have an adverse effect in terms of tissue damage observed at histology. However, previous work from our lab has shown that at high-pressure exposures, hemorrhage can be observed throughout the focal region (Fletcher et al. 2020b). Increasing the burst length can potentially affect the usefulness of SBPK FUS in mitigating formation of standing waves in human vertebrae, but benchtop experiments show that this can be accounted for by decreasing the BRF.

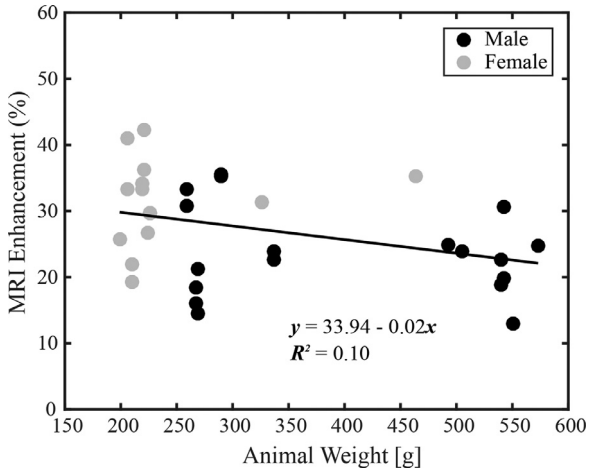


Fig. 15. Relationship between magnetic resonance imaging enhancement and animal weight for locations treated using the control sonication parameters. The plot also indicates the biological sex of the animal for each data point.

Increasing the treatment duration and the BRF corresponded to increased MRI enhancement, but these changes were not statistically significant (treatment duration: $p = 0.056$; BRF: $p = 0.064$). A treatment duration of 300 s showed no increased incidence of moderate or extensive damage at histology compared with the control treatment duration of 120 s. This increasing trend is in agreement with previous studies using longer pulse exposures (Chopra et al. 2010). According to the U.S. Food and Drug Administration injection label, Definity microbubbles have a mean half-life of 1.3 min (78 s) in healthy circulation, but this value will vary for each individual, and bubbles may remain in circulation beyond this point. Considering the half-life, a 120 s treatment duration should be sufficient. However, the data presented here indicate that there may be some benefit to increasing the treatment duration, although there was comparatively high variability in the MRI enhancement at locations treated for 300 s (Fig. 9b). In this study, microbubbles were administered as a bolus, but previous studies of BBBO have shown that slow microbubble infusion improves consistency and reduces damage relative to bolus administration (O'Reilly et al. 2011; Lapin et al. 2020). Previous studies have also noted that microbubble infusions may improve the efficacy of feedback control algorithms based on acoustic emissions by modulating the microbubble concentration in circulation along with the FUS exposure, to avoid decreasing microbubble concentrations over the treatment duration (Sun et al. 2017b). Informed by the results of this and previous studies, future work may be done to tailor sonication length and injection protocol with the goal of consistently achieving more efficient BSCBO.

While no statistically significant changes in MRI enhancement were observed after an increase in BRF from 20 to 40 kHz, there were differences in the extent of tissue damage observed at histology. Four of eight locations treated with the higher BRF, across three of the four animals in this group, were scored at histology grade 2 (moderate damage), compared with just one of eight locations treated with the control BRF. This result is in disagreement with a previous study (O'Reilly et al. 2011) which showed statistically significant increases in enhancement with BRF without adverse effects observed at histology, using short burst exposures. The main difference between the exposures in that study and in the present study is the phase shifts that are applied at the start of each burst in SBPK exposures. It is possible that at higher BRFs, bubble response is such that in the "off-time" following a burst, bubbles are still undergoing residual, sustained cavitation. At the time of the subsequent burst, the bubbles are forced to oscillate at a different phase, potentially leading to non-uniform oscillations and damage to the bubble shells and increasing the likelihood of damage to the vascular walls.

Lower BRFs may be advantageous, as they allow enough time for the bubbles to cease cavitating before the subsequent burst is applied.

In this study, there was no difference in enhancement observed between locations treated with 2 ms and 10 ms pulse lengths ($p = 0.912$). Previous work in the brain using long, sinusoidal pulses has shown that longer pulse lengths correspond to increased levels of BBBO (McDannold et al. 2008), despite earlier work showing no difference between pulses of 10 and 100 ms (Hynynen et al. 2001). A possible reason for the discrepancy with the results presented here is that because of the "off-time" during the SBPK pulse, if the bubble shells are damaged, they will dissolve more quickly. This hypothesis is supported by a drop in acoustic emissions at the second harmonic. Conversely, previous work using long burst exposures has shown sustained emissions at the subharmonic (Jones et al. 2020). In the long-burst case, the bubble is being driven acoustically during the entire burst, which may sustain it. Although there appears to be no disadvantage to using greater pulse lengths, reducing the pulse length could allow for more interleaved locations to be treated within the pulse repetition period, ultimately allowing faster and more efficient treatment of a larger region of tissue.

Although there was a difference in MRI enhancement between male and female animals ($p = 0.037$), there was also a statistically significant difference in weight between the two groups ($p = 0.006$). To achieve a clearer understanding of the effect of biological sex, it may be necessary to perform experiments in a cohort of animals where their weight is strictly limited.

Evans blue dye was injected after the FUS treatments and was allowed to circulate for 2 h before animal perfusion and sacrifice. In previous studies, extravasation of Evans blue dye after ultrasound-induced BSCBO has been quantified using spectroscopy (Montero et al. 2019). However, using such techniques requires sectioning and processing of the spinal cord in a manner that makes subsequent histologic analysis impossible or extremely difficult (Montero et al. 2019). Further, as dye leakage occurs to a greater degree in gray matter than in white (McDannold et al. 2012; Fletcher et al. 2020a), even a robust qualitative analysis of Evans blue extravasation would rely on spinal cord dissection, which would limit the potential for histologic analysis. In this study, hematoxylin and eosin histologic staining was used as the primary marker of the effect-modifying pulse parameters on tissue damage. Therefore, Evans blue extravasation was treated not as an indicator of treatment outcome but rather as a potential confirmation of BSCBO and a marker to locate treatment locations at tissue harvesting.

Limitations of this study include the small sample size in each treatment group and the variable ultrasound transmission to the spinal cord. Only four animals were included in each group, with four to eight data points per parameter value. For two parameters (treatment duration and BRF), changes in MRI enhancement were observed but the threshold of statistical significance was not met. In addition to animal weight, differences in spinal alignment could affect the *in situ* ultrasound field and pressure. At clinical scale, flexion of the spinal column in the sagittal plane can lead to increased levels of ultrasound delivery owing to the increased spaces between individual vertebrae, resulting in larger acoustic windows (Xu and O'Reilly 2020). Further investigations would be necessary to understand the effect of differences in spinal alignment on FUS transmission to the spinal cord, particularly in small-animal models. Previous work from our group has shown variable FUS transmission along the length of the vertebral arch (O'Reilly et al. 2018; Fletcher et al. 2020a). While we accounted for intra-animal variability by investigating both control and test parameters in each animal, inter-animal variabilities were observed and may affect the study findings. Because fixed pressures were used in this study, the variability in ultrasound transmission in some animals and at some locations may have resulted in FUS over-exposure owing to the under-estimation of *in situ* pressures. This reiterates the need for a feedback controller based on acoustic emissions to promote safe BSCBO (O'Reilly and Hynynen 2012; Sun et al. 2017b; Fletcher et al. 2020b).

Based on the results of this study, it will be beneficial to increase the burst length and decrease the BRF in future studies of BSCBO using SBPK FUS exposures. This should increase the efficacy of BSCBO without compromising the usefulness of SBPK for mitigating standing waves. Despite not meeting the threshold for statistical significance, increasing the treatment duration may also lead to increased efficacy in drug delivery applications without adverse tissue effects at histology. Future work should include the investigation of microbubble response to SBPK exposures, to gain insight into the results observed in the pulse length group.

## CONCLUSION

Different pulsing parameters for SBPK FUS—including pressure, treatment duration, pulse length, BRF and burst length—were investigated for their efficacy in BSCBO and their likelihood of resulting in tissue damage. Increased acoustic pressure corresponded to increased MRI enhancement, with successful opening at all locations at or above 0.28 MPa (*in situ* estimate). Increased burst length led to a statistically significant increase in MRI enhancement without increased damage observed at histology. Adjusting the design of SBPK FUS exposures to incorporate these results may lead to improved drug delivery across the BSCB for the treatment of spinal cord diseases and disorders.

*Acknowledgments*—The authors would like to thank the following people who contributed to this study: Natalia Ogrodnik, who provided veterinary care and experimental assistance; Viva Chan and Shawna Rideout-Gros, who assisted with veterinary care; Marc Santos, who provided experimental assistance; Jennifer Sun, who was responsible for histologic processing; Dallan McMahon, who assisted with data analysis; and Ryan Jones, who provided general assistance and scientific expertise. Support for this work was provided by the Terry Fox Research Institute New Investigator Award program, the Ontario Ministry of Research, Innovation and Science Early Researcher Award, the Canada Foundation for Innovation John Evans Leaders Fund and the Canada Research Chair program.

*Conflict of interest disclosure*—The authors have no conflicts of interest to declare.

## REFERENCES

Abrahao A, Meng Y, Llinas M, Huang Y, Hamani C, Mainprize T, Aubert I, Heyn C, Black SE, Hynynen K, Lipsman N, Zinman L. First-in-human trial of blood−brain barrier opening in amyotrophic lateral sclerosis using MR-guided focused ultrasound. Nat Commun 2019;10:1–9.

Aryal M, Arvanitis CD, Alexander PM, McDannold N. Ultrasound-mediated blood−brain barrier disruption for targeted drug delivery in the central nervous system. Adv Drug Deliv Rev 2014;72:94–109.

Baron C, Aubry JF, Tanter M, Meairs S, Fink M. Simulation of intracranial acoustic fields in clinical trials of sonothrombolysis. Ultrasound Med Biol 2009;35:1148–1158.

Bartanusz V, Jezova D, Alajajian B, Digicaylioglu M. The blood-spinal cord barrier: Morphology and clinical implications. Ann Neurol 2011;70:194–206.

Carpentier A, Canney M, Vignot A, Reina V, Beccaria K, Horodyckid C, Karachi C, Leclercq D, Lafon C, Chapelon J, Capelle L, Cornu P, Sanson M, Hoang-xuan K. Clinical trial of blood-brain barrier disruption by pulsed ultrasound. Science Translational Medicine 2016;8:343re2−343re2 .

Choi JJ, Pernot M, Small SA, Konofagou EE. Noninvasive, transcranial and localized opening of the blood-brain barrier using focused ultrasound in mice. Ultrasound Med Biol 2007;33:95–104.

Choi JJ, Selert K, Gao Z, Samiotaki G, Baseri B, Konofagou EE. Noninvasive and localized blood-brain barrier disruption using focused ultrasound can be achieved at short pulse lengths and low pulse repetition frequencies. J Cereb blood flow Metab 2011;31:725–737.

Chopra R, Vykhodtseva N, Hynynen K. Influence of exposure time and pressure amplitude on blood-brain-barrier opening using transcranial ultrasound exposures. ACS Chem Neurosci 2010;1:391–398.

Daffertshofer M, Gass A, Ringleb P, Sitzer M, Sliwka U, Els T, Sedlaczek O, Koroshetz WJ, Hennerici MG. Transcranial low-frequency ultrasound-mediated thrombolysis in brain ischemia: Increased risk of hemorrhage with combined ultrasound and tissue plasminogen activator—results of a phase II clinical trial. Stroke 2005;36:1441–1446.

Daneman R, Prat A. The blood−brain barrier. Cold Spring Harb Perspect Biol 2015;7 a020412.

Fletcher SMP, Choi M, Ogrodnik N, O'Reilly MA. A porcine model of transvertebral ultrasound and microbubble-mediated blood-spinal cord barrier opening. Theranostics 2020a;10:7758–7774.

Fletcher SMP, Ogrodnik N, O'Reilly MA. Enhanced detection of bubble emissions through the intact spine for monitoring ultrasound-mediated blood-spinal cord barrier opening. IEEE Trans Biomed Eng 2020b;67:1387–1396.

Fletcher SMP, O'Reilly MA. Analysis of multifrequency and phase keying strategies for focusing ultrasound to the human vertebral canal. IEEE Trans Ultrason Ferroelectr Freq Control 2018;65:2322–2331.

Hynynen K, McDannold N, Sheikov NA, Jolesz FA, Vykhodtseva N. Local and reversible blood-brain barrier disruption by noninvasive focused ultrasound at frequencies suitable for trans-skull sonications. Neuroimage 2005;24:12–20.

Hynynen K, McDannold N, Vykhodtseva N, Jolesz FA. Noninvasive MR imaging-guided focal opening of the blood-brain barrier in rabbits. Radiology 2001;220:640–646.

Jones RM, McMahon D, Hynynen K. Ultrafast three-dimensional microbubble imaging in vivo predicts tissue damage volume distributions during nonthermal brain ablation. Theranostics 2020;10:7211–7230.

Jordão JF, Ayala-Grosso CA, Markham K, Huang Y, Chopra R, McLaurin J, Hynynen K, Aubert I. Antibodies targeted to the brain with image-guided focused ultrasound reduces amyloid-$\beta$ plaque load in the TgCRND8 mouse model of Alzheimer's disease. PLoS One 2010;5:e10549.

Kinoshita M, McDannold N, Jolesz FA, Hynynen K, Dunn F. Noninvasive localized delivery of herceptin to the mouse brain by MRI-guided focused ultrasound-induced blood−brain barrier disruption. Proc Natl Acad Sci 2006;103:11719–11723.

Lapin NA, Gill K, Shah BR, Chopra R. Consistent opening of the blood brain barrier using focused ultrasound with constant intravenous infusion of microbubble agent. Sci Rep 2020;10:16546.

Lipsman N, Meng Y, Bethune AJ, Huang Y, Lam B, Masellis M, Herrmann N, Heyn C, Aubert I, Boutet A, Smith GS, Hynynen K, Black SE. Blood-brain barrier opening in Alzheimer's disease using MR-guided focused ultrasound. Nat Commun 2018;9:1–7.

Mainprize T, Lipsman N, Huang Y, Meng Y, Bethune A, Ironside S, Heyn C, Alkins R, Trudeau M, Sahgal A, Perry J, Hynynen K. Blood-brain barrier opening in primary brain tumors with non-invasive MR-guided focused ultrasound: A clinical safety and feasibility study. Sci Rep 2019;9:321.

McDannold N, Arvanitis CD, Vykhodtseva N, Livingstone MS. Temporary disruption of the blood-brain barrier by use of ultrasound and microbubbles: Safety and efficacy evaluation in rhesus macaques. Cancer Res 2012;72:3652–3666.

McDannold N, Vykhodtseva N, Hynynen K. Effects of acoustic parameters and ultrasound contrast agent dose on focused-ultrasound induced blood-brain barrier disruption. Ultrasound Med Biol 2008;34:930–937.

McDannold N, Zhang Y, Vykhodtseva N. The effects of oxygen on ultrasound-induced blood-brain barrier disruption in mice. Ultrasound Med Biol 2017;43:469–475.

Montero AS, Bielle F, Goldwirt L, Lalot A, Bouchoux G, Canney M, Belin F, Beccaria K, Pradat PF, Salachas F, Boill S, Lafon C, Chapelon JY, Carpentier A. Ultrasound-induced blood-spinal cord barrier opening in rabbits. Ultrasound Med Biol 2019;45:2417–2426.

O'Reilly MA, Chinnery T, Yee M, Wu S, Hynynen K, Kerbel R, Jan G, Pritchard K, Sahgal A. Preliminary investigation of focused ultrasound-facilitated drug delivery for the treatment of leptomeningeal metastases. Sci Rep 2018;8:1–8.

O'Reilly MA, Hynynen K. Blood-brain barrier: Real-time feedback-controlled focused ultrasound disruption by using an acoustic emissions-based controller. Radiology 2012;263:96–106.

O'Reilly MA, Waspe AC, Ganguly M, Hynynen K. Focused-ultrasound disruption of the blood-brain barrier using closely-timed short pulses: Influence of sonication parameters and injection rate. Ultrasound Med Biol 2011;37:587–594.

Pardridge WM. The blood-brain barrier: Bottleneck in brain drug development. NeuroRx 2005;2:3–14.

Payne AH, Hawryluk GW, Anzai Y, Odéen H, Ostlie MA, Reichert EC, Stump AJ, Minoshima S, Cross DJ. Magnetic resonance imaging-guided focused ultrasound to increase localized blood-spinal cord barrier permeability. Neural Regen Res 2017;12:2045–2049.

Rothman KJ. No adjustments are needed for multiple comparisons. Epidemiology 1990;1:43–46.

Simpson DH, Ting Chin C, Burns PN. Pulse inversion doppler: A new method for detecting nonlinear echoes from microbubble contrast agents. IEEE Trans Ultrason Ferroelectr Freq Control 1999;46:372–382.

Sun T, Sutton JT, Power C, Zhang Y, Miller EL, McDannold NJ. Transcranial cavitation-mediated ultrasound therapy at sub-MHz

frequency via temporal interference modulation. Appl Phys Lett 2017a;111:1–4.
Sun T, Zhang Y, Power C, Alexander PM, Sutton JT, Aryal M, Vykhodtseva N, Miller EL, Mcdannold NJ. Closed-loop control of targeted ultrasound drug delivery across the blood-brain/tumor barriers in a rat glioma model. Proc Natl Acad Sci 2017b;114:E10281–E10290.
Wachsmuth J, Chopra R, Hynynen K. Feasibility of transient image-guided blood-spinal cord barrier disruption. AIP Conf Proc 2009;1113:256–259.
Weber-Adrian D, Thevenot E, O'Reilly MA, Oakden W, Akens MK, Ellens N, Markham-Coultes K, Burgess A, Finkelstein J, Yee AJM, Whyne CM, Foust KD, Kaspar BK, Stanisz GJ, Chopra R, Hynynen K, Aubert I. Gene delivery to the spinal cord using MRI-guided focused ultrasound. Gene Ther 2015;22:568–577.
Xu R, O'Reilly MA. A spine-specific phased array for transvertebral ultrasound therapy: Design and simulation. IEEE Trans Biomed Eng 2020;67:256–267.